Role of chirality in angular momentum coupling for $A\sim130$ odd-odd triaxial nuclei: ^{132}La

K. Starosta, C. J. Chiara,* D. B. Fossan, T. Koike, T. T. S. Kuo, and D. R. LaFosse
Department of Physics and Astronomy, State University of New York at Stony Brook, Stony Brook, New York 11794-3800

S. G. Rohoziński
Institute of Theoretical Physics, Warsaw University, Hoża 69, PL-00-681 Warsaw, Poland

Ch. Droste, T. Morek, and J. Srebrny
Institute of Experimental Physics, Warsaw University, Hoża 69, PL-00-681 Warsaw, Poland
(Received 6 November 2001; published 5 April 2002)

Nearly degenerate partner bands observed in $A\sim130$ odd-odd triaxial nuclei are interpreted as a manifestation of chirality in the intrinsic reference frame. A phenomenological approach, based on a core-particle-hole coupling model, has been developed to address the experimental observables. This laboratory-frame model, in which chiral symmetry has been restored, includes a triaxial core, a particle/hole single-particle Hamiltonian, and quadrupole-quadrupole interactions. The optimal model parameters are investigated. The results of the calculations indicate the existence of pairs of $\pi h_{11/2}\nu^{-1}h_{11/2}$ states with the same spin, parity, and similar excitation energy forming partner bands that are nearly degenerate over a range of spins. These calculated partner bands are consistent with the chiral band interpretation and are in agreement with experimental observations in this region. This model has been applied to excited states in ^{132}La, which have been studied via the ^{123}Sb(^{13}C,4n) reaction using γ-ray spectroscopic techniques. In addition to the yrast $\pi h_{11/2}\nu^{-1}h_{11/2}$ band, the partner band was observed with experimental properties consistent with the same $\pi h_{11/2}\nu^{-1}h_{11/2}$ configuration. These doublet bands resemble those observed systematically for several $N=75$ isotones of ^{132}La.

DOI: 10.1103/PhysRevC.65.044328 PACS number(s): 21.10.Re, 21.60.−n, 23.20.Lv, 27.60.+j

I. INTRODUCTION

Recent experimental investigations of odd-odd nuclei in the $A\sim130$ region [1–5] have resulted in the observation of systematic doublet bands built on unique-parity $h_{11/2}$ valence proton and neutron orbitals. These structures are interpreted as a manifestation of chirality in the angular momentum coupling, which had been predicted in Ref. [6]. In the $Z\sim57$ and $N\sim75$ region, the Fermi level is in the lower part of the $h_{11/2}$ proton subshell, but in the higher part of the $h_{11/2}$ neutron subshell.[1] Model calculations for a triaxial potential [6,7] indicate that the angular momentum for an orbital in the lower part of a high-j subshell is oriented along the short axis of the triaxial core while for an orbital in the higher part of the subshell, the orientation is along the long axis. Such orientations result in a maximal overlap of the core wave function with the particlelike wave function and a minimal overlap with the holelike wave function; in both cases, the overlap results in a decrease in energy due to the attractive nature of the nuclear force. The angular momentum of the core itself is oriented along the intermediate axis, which corresponds to the largest value for irrotational-flow-like moment of inertia [7,8], thus minimizing the rotational energy. These three mutually perpendicular angular momenta can be arranged to form two systems with opposite chirality, left- and right-handedness, as shown in Fig. 1, representing the breaking of chiral symmetry in the intrinsic frame of the nucleus. These systems cannot be transformed into each other by rotation or space inversion, but are related by an operator that involves time reversal.[2] This can be visualized with the use of Fig. 1 following the fact that the time-reversal operator reverses the orientation of each of the angular momentum vectors.

In this paper, such chirality for an odd-odd triaxial nucleus is studied theoretically with the use of a phenomenological core-particle-hole coupling model formulated in the laboratory reference frame, where chiral symmetry is restored. The model is developed from a Hamiltonian with quadrupole-quadrupole nuclear interactions following an approach presented for odd-even nuclei in Refs. [9–11]. The eigenvalues of the Hamiltonian are found using the Kerman-Klein-Dönau-Frauendorf method (for a recent review, see Ref. [12] and references therein); a similar model was analyzed in Ref. [13]. The triaxial core is introduced into the calculations via reduced $E2$ matrix elements and energy spectra; the parameters fitted to reproduce the properties of even and odd neighbors are directly applicable to the calculations for odd-odd nuclei. For these calculations, the triaxial

*Present address: Department of Chemistry, Washington University, St. Louis, Missouri 63130.

[1]Following this fact and the model calculations presented below, the configuration for the doublet bands discussed in the current work is labeled $\pi h_{11/2}\nu^{-1}h_{11/2}$ throughout the paper.

[2]Such a chiral operator may be defined as a combination of time reversal and rotation by 180° around an axis perpendicular to the quantization axis. The convention that follows Ref. [8] with the z and y axes chosen as the quantization and rotation axes, respectively, is widely accepted.

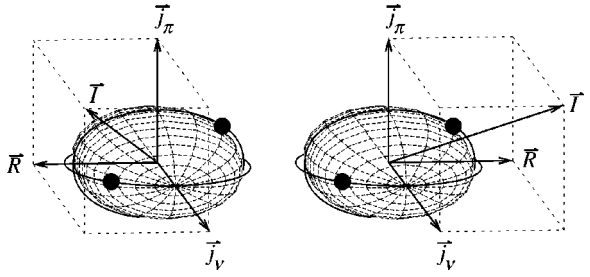

FIG. 1. Two possible couplings of the three angular momenta in a triaxial odd-odd nucleus to the total angular momentum $\vec{I}$. In the $A\sim130$ region, the three mutually perpendicular angular momenta involved are those for the proton $h_{11/2}$ particle ($\vec{j}_\pi$), for the neutron $h_{11/2}$ hole ($\vec{j}_\nu$), and for the core ($\vec{R}$).

rotor of Ref. [14] is employed for the core. The angular momenta coupling of the valence proton, valence neutron, and the core rotation are analyzed via the resulting wave functions from these model calculations by evaluating expectation values of scalar products of the three angular momentum operators; deduced orientations of the angular momenta allow the exploration of the chiral aplanar condition for the total angular momentum. The approach presented here is complementary to the study of chirality from the intrinsic body-fixed reference frame using the microscopic Tilted Axis Cranking (TAC) model of Refs. [15,6], which predicts triaxial shapes with $\gamma\sim30°$ and aplanar minima for $\pi h_{11/2}\nu^{-1}h_{11/2}$ routhians in the $A\sim130$ region.

The orthogonal coupling of three angular momentum vectors violates time-reversal invariance. It should be noted, however, that the nuclear Hamiltonian, in the laboratory reference frame, is invariant with respect to time reversal. For specific configurations, states with defined chirality are possible only in the intrinsic body-fixed reference frame. For such states in the intrinsic reference frame, the required restoration of time-reversal invariance in the laboratory reference frame results in the doubling of states forming nearly degenerate partner bands. Since the core rotational contribution to the total angular momentum varies along the rotational band, the near degeneracy is expected to exist only within a limited spin/rotational frequency range where the three vectors of interest are comparable in magnitude. The wave functions for the doublet states provided by the model in the laboratory reference frame are those linear combinations of the wave functions for the left-handed and right-handed systems in the intrinsic reference frame, which are invariant under time reversal.

These model calculation investigations in the laboratory frame are applied to doublet bands built on the $\pi h_{11/2}\nu^{-1}h_{11/2}$ configuration observed in the $N=75$ triaxial ^{132}La nucleus. Partial results of this work have been given in Ref. [16]. The experimental study of ^{132}La will be presented in the next section followed by the development of the core-particle-hole coupling model and its application to the experimental results.

II. EXPERIMENTAL METHOD AND RESULTS

Excited states in ^{132}La were populated with the ^{123}Sb(^{13}C,4n) reaction at a beam energy of 64 MeV. The

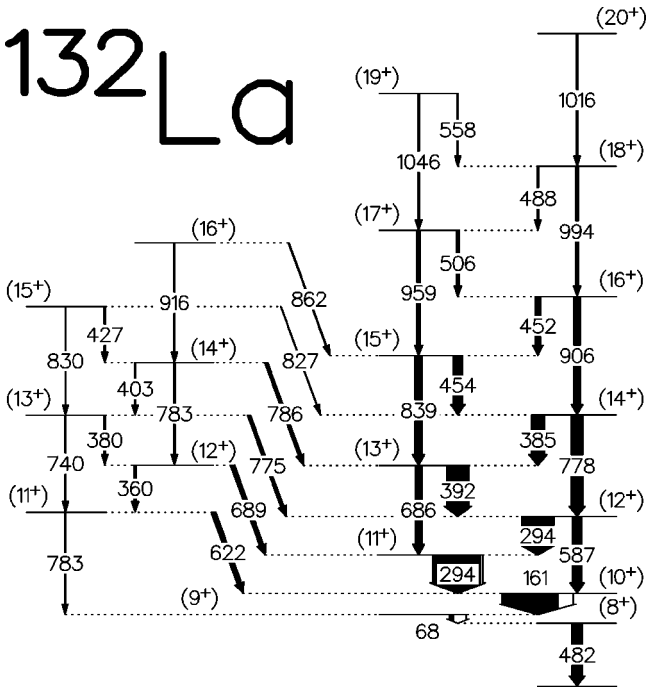

FIG. 2. Partial level scheme for ^{132}La. The widths of the arrows represent the relative intensity of the γ-ray transitions with the internal conversion contribution indicated by the white component of the arrow. Energies are given in keV.

beam was provided by the tandem-injected superconducting LINAC of the Nuclear Structure Laboratory at the State University of New York at Stony Brook. The ^{123}Sb target was 2 mg/cm^2 thick and backed with 16 mg/cm^2 natural Pb. The experimental setup consisted of six Compton-suppressed Ge detectors working in conjunction with a 14-element BGO multiplicity filter. The detectors were placed at approximately $\pm30°$, $\pm90°$, and $\pm150°$ relative to the beam direction. The γ-ray energy resolution measured at $\sim$550 keV was full width at half-maximum $\sim$2.2 keV. A total of $\sim82\times10^6$ time-gated prompt γ-γ coincidence events were collected in this experiment. Coincident γ-ray events were sorted into an E_γ-E_γ matrix and analyzed using the γ-ray spectroscopy software package RADWARE [17]. A partial level scheme presenting the yrast band built on the $\pi h_{11/2}\nu^{-1}h_{11/2}$ configuration identified in a previous study [18], and the partner band observed in the current study, is shown in Fig. 2. Figure 3 presents the γ-ray spectrum created from a gate on the 380-keV intraband transition of the partner band. The number of counts in the peak for the 689-keV linking transition in this spectrum compared to the number of counts for the 360-keV partner-band member indicates, when corrected for efficiency (see Table I for details), a significant decay out from the partner band into the yrast band.

A Direction Correlation from Oriented states (DCO) study [19] was performed to determine γ-ray multipolarities. An asymmetric DCO matrix was sorted with the detectors at $\theta\approx30°$ and $\theta\approx150°$ incremented on one axis and the detectors with $\theta\approx90°$ on the other axis. DCO ratios [19] extracted for known quadrupole-dipole and quadrupole-quadrupole co-

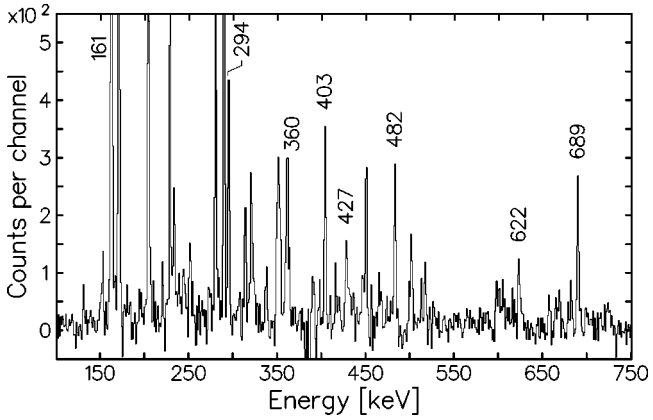

FIG. 3. Coincidence spectrum gated on the 380-keV γ-ray transition. Those transitions reported in Fig. 2 are labeled with their energies in keV; the other peaks correspond to transitions depopulating the (8^+) state of the yrast band.

incident γ rays in ^{132}La [18] are $R_{DCO}=0.57(9)$ for the 587–482 keV cascade and $R_{DCO}=0.97(15)$ for the 778–587 keV cascade. Energies, intensities, DCO ratios, proposed spin assignments for the observed excited levels, and multipolarities for the γ-ray transitions are listed in Table I.

The experimental values of the DCO ratios extracted for the quadrupole-dipole cascades were used to calculate the mixing ratio δ for the $M1/E2$ intraband transitions in the yrast band [19]. These mixing ratios are of the order of ~ 0.1 when a reasonable spin alignment parameter $\sigma/I=0.3$ is assumed. The DCO analysis for the transitions linking the partner band and the yrast band was performed with the R_{DCO} measured in gates set on strong $M1/E2$ transitions in the yrast band. DCO ratios ~ 1.5 were measured for the 622-, 689-, 775-, and 786-keV γ rays using gates set on the 161- and 294-keV mixed dipole transitions. This rules out an $E1$ assignment for the links since the values calculated for stretched and nonstretched $E1$ transitions are $R_{DCO}\leqslant 1.2$ and $R_{DCO}\leqslant 0.6$, respectively. A stretched $E2$ hypothesis is also ruled out due to the expected $R_{DCO}\sim 0.5$. The same is true for an $I_i^{\pi}=I_f^{\pi}$ mixed $M1/E2$ assignment since the calculations give $R_{DCO}\leqslant 1$ for any mixing ratio considered. Therefore, the above four links are all of mixed $\Delta I=1$ $M1/E2$ character with a mixing ratio $\delta\approx -0.3$. This yields positive parity for the partner band and the relative spins as shown in Fig. 2. The proposed assignment is consistent with that determined for ^{136}Pm in Ref. [4]; the $\Delta I=1$ $M1/E2$ multipolarity for the linking transitions in this work results, in addition to the DCO analysis, from the polarization measurement.

The existence of mixed $M1/E2$ links between the yrast and partner band suggests strongly that the partner band is built on the same unique-parity orbitals as the yrast band. The only other positive-parity configurations at low excitation energy which are possible in odd-odd nuclei in the $A\sim 130$ region involve positive-parity proton and positive-parity neutron orbitals. However, the selection rules for the $M1$ and $E2$ operators yield vanishing matrix elements between such configurations and the yrast band built on negative-parity orbitals. As a consequence, the links should be strongly hindered unless the partner band is built on the $\pi h_{11/2}\nu^{-1}h_{11/2}$ configuration as well.

The current experimental data yield relative spin assignments only; absolute spin assignments for the bands of interest have to rely on the results of the previous study. The $\pi h_{11/2}\nu^{-1}h_{11/2}$ band in ^{132}La was proposed in Ref. [18] to decay to an isomeric state with a $t_{1/2}=24.3$ min half-life. A spin and parity (6^-) for this state was assigned in Ref. [20] based on an electron conversion measurement for the observed depopulating γ-ray transitions. The same assignment was preferred in Ref. [21] in which the results of an atomic-beam magnetic resonance measurement are discussed. The 482-keV transition linking the partner bands to the isomeric state was assigned a stretched $E1$ multipolarity based on angular distribution measurements [18] that resulted in the (7^+) assignment for the bandhead of the yrast band.

A systematic study of the bands built on the $\pi h_{11/2}\nu h_{11/2}$ configuration in the odd-odd $A\sim 130$ nuclei was reported in Ref. [22] in which new spin assignments for several bands were suggested; it was based on the assumption that the excitation energy of the levels with the same spin in a chain of deformed odd-odd isotopes and isotones varies in a smooth way. This study includes the $\pi h_{11/2}\nu^{-1}h_{11/2}$ bands in the $N=75$ isotones, where spin assignments higher by one unit of $\hbar$ were proposed in ^{132}La, ^{134}Pr, and ^{136}Pm as compared to the original assignments proposed in Refs. [18], [23], and [24], respectively. The spin assignment in ^{130}Cs proposed in Ref. [25] was treated as a reference point and, therefore, not altered in this study.

These ambiguities in the spin assignment may be attributed to well-known difficulties with experimental studies of odd-odd nuclei. The spins proposed in Ref. [22] with the (8^+) assignment for the bandhead of the yrast band in ^{132}La were found to be in better agreement with the results of the calculations discussed in Sec. IV C and are therefore adopted in the present paper.

III. THE CORE-PARTICLE COUPLING MODEL

A. The Hamiltonian

For the purpose of the current study, the total nuclear Hamiltonian is assumed to consist of a spherically symmetric mean-field Hamiltonian and a quadrupole-quadrupole interaction term, namely,

$$H=\sum_{\tau,\alpha}\varepsilon_{\tau\alpha}a^{\dagger}_{\tau\alpha}a_{\tau\alpha}-\frac{1}{2}\sum_{\tau,\tau'}\chi_{\tau\tau'}\sum_{m}Q^{\dagger}_{m}(\tau)Q_{m}(\tau'), \quad (1)$$

where $\varepsilon_{\tau\alpha}$ denotes the energy for the single-particle state $|\alpha\rangle$, α is the set of the quantum numbers $(j_{\alpha},m_{\alpha},n_{\alpha},l_{\alpha})$ for the single-particle state $|\alpha\rangle$, and τ,τ' are indices that run over both protons and neutrons. Two indices $(\tau,\ \tau')$ are required for the two-body interaction term. The symbol $Q(\tau)$ denotes the quadrupole operator of protons or neutrons defined as

$$Q_m(\tau)=\frac{1}{\sqrt{5}}\sum_{\sigma_{\tau\alpha},\sigma_{\tau\alpha'}}q(\sigma_{\tau\alpha},\sigma_{\tau\alpha'})[a^{\dagger}_{\tau\alpha}\tilde{a}_{\tau\alpha'}]_{2m}, \quad (2)$$

TABLE I. Properties of γ-ray transitions observed in the current study.

E_γ [a] (keV)	I_γ (%)	DCO ratio	I_i^π	→	I_f^π	Multipolarity
67.6			(9^+)	→	(8^+)	$M1/E2$
161.3	100.0(3.0)	0.64(6) [b]	(10^+)	→	(9^+)	$M1/E2$
293.6	140.0(4.0)	0.46(6) [c]	(11^+)	→	(10^+)	$M1/E2$
293.5			(12^+)	→	(11^+)	$M1/E2$
360.1	4.1(0.1)		(12^+)	→	(11^+)	$M1/E2$
380.0	2.1(0.1)		(13^+)	→	(12^+)	$M1/E2$
385.3	23.3(0.7)	0.42(5) [b]	(14^+)	→	(13^+)	$M1/E2$
392.1	39.1(1.2)	0.58(5) [b]	(13^+)	→	(12^+)	$M1/E2$
402.7	2.7(0.1)		(14^+)	→	(13^+)	$M1/E2$
426.9	>1.0		(15^+)	→	(14^+)	$M1/E2$
451.9	9.1(0.3)	0.35(6) [b]	(16^+)	→	(15^+)	$M1/E2$
453.6	16.6(0.5)		(15^+)	→	(14^+)	$M1/E2$
481.7	18.6(0.6)	0.57(9) [b]				$E1$
487.5	1.9(0.1)		(18^+)	→	(17^+)	$M1/E2$
506.3	4.4(0.1)	0.5(2) [b]	(17^+)	→	(16^+)	$M1/E2$
558.0	1.4(0.1)		(19^+)	→	(18^+)	$M1/E2$
587.3	16.2(0.5)		(12^+)	→	(10^+)	$E2$
622.0	8.0(0.3)	1.7(3) [d]	(11^+)	→	(10^+)	$M1/E2$
686.1	11.6(0.4)		(13^+)	→	(11^+)	$E2$
688.6	7.4(0.2)	1.4(2) [e]	(12^+)	→	(11^+)	$M1/E2$
740.2	1.2(0.1)		(13^+)	→	(11^+)	$E2$
774.7	5.4(0.2)	1.5(2) [e]	(13^+)	→	(12^+)	$M1/E2$
777.9	19.9(0.6)	0.97(15) [b]	(14^+)	→	(12^+)	$E2$
783.0	1.9(0.1)		(14^+)	→	(12^+)	$E2$
783.3	0.7(0.4)		(11^+)	→	(9^+)	$E2$
785.5	5.3(0.2)	1.8(3) [e]	(14^+)	→	(13^+)	$M1/E2$
827.0	1.0(0.1)		(15^+)	→	(14^+)	$M1/E2$
829.8	>0.5		(15^+)	→	(13^+)	$E2$
839.2	11.9(0.4)		(15^+)	→	(13^+)	$E2$
862.2	1.6(0.1)		(16^+)	→	(15^+)	$M1/E2$
906.0	11.8(0.4)		(16^+)	→	(14^+)	$E2$
915.6	1.4(0.1)		(16^+)	→	(14^+)	$E2$
958.8	5.1(0.2)		(17^+)	→	(15^+)	$E2$
994.3	4.4(0.2)		(18^+)	→	(16^+)	$E2$
1015.6	2.8(0.1)		(20^+)	→	(18^+)	$E2$
1046.3	2.6(0.1)		(19^+)	→	(17^+)	$E2$

[a]Energies are typically accurate to within ± 0.3 keV.
[b]Gated on 587-keV $E2$ transition.
[c]Gated on 778-keV $E2$ transition.
[d]Gated on 161-keV mixed $M1/E2$ transition.
[e]Gated on 294-keV mixed $M1/E2$ transitions.

where $\sigma_{\tau\alpha}=(j_\alpha,n_\alpha,l_\alpha)$ denotes the set of the quantum numbers for the single-particle state $|\alpha\rangle$ without the magnetic quantum number m_α for $\tau=\pi$ or $\tau=\nu$, respectively. The symbol $q(\sigma_{\tau\alpha},\sigma_{\tau\alpha'})$ denotes the reduced matrix element of the single-particle quadrupole operator calculated between states $|\alpha\rangle$ and $|\alpha'\rangle$. The phase convention for a single-particle wave function as defined in Sec. 3-A of Ref. [8] is adopted throughout this paper. With this phase convention

$$Q_m^\dagger(\tau)=(-)^m Q_{-m}(\tau) \tag{3}$$

and the reduced matrix elements

$$q(\sigma_{\tau\alpha},\sigma_{\tau\alpha'})=(-)^{j_\alpha-j_{\alpha'}}q(\sigma_{\tau\alpha'},\sigma_{\tau\alpha}) \tag{4}$$

are real. The symbol $[a^\dagger_{\tau\lambda}\tilde{a}_{\tau\mu}]_{LM}$ denotes the coupling of spherical tensors, in this case the creation operators for a particle in orbital $|\lambda\rangle$ and a hole in orbital $|\mu\rangle$, to a state with angular momentum LM

$$[a^\dagger_{\tau\lambda}\tilde{a}_{\tau\mu}]_{LM}=\sum_{m_\lambda,m_\mu}\langle j_\lambda m_\lambda j_\mu m_\mu|LM\rangle a^\dagger_{\tau\lambda}\tilde{a}_{\tau\mu}. \tag{5}$$

The above Hamiltonian does not include pairing correlations; however, this simplification is justified by the fact that the model is applied to very specific bands in the $A\sim130$ region built on valence nucleons occupying $h_{11/2}$ orbitals. In this paper, nuclei with $Z\sim57$ and $N\sim75$ are considered, where the Fermi level is low compared to the $\pi h_{11/2}$ subshell while high compared to the $\nu h_{11/2}$ subshell. In such cases, a simplified model treating the valence proton as a pure particle and the valence neutron as a pure hole is expected to approximate with sufficient accuracy the quasiparticle model, which includes pairing. In the current approach, the pairing interactions for all the core nucleons are considered to be core properties. Indeed, these are the interactions that result in a irrotational-flow-like behavior for the triaxial-core moments of inertia discussed in Sec. IV A. An analogous model with pairing interactions for odd-even nuclei is described in Refs. [9–11] and references therein.

B. Wave functions for core-particle, -hole, and -particle-hole coupling model

For core-particle coupling, the wave function of a state with angular momentum IK (see footnote 3) and additional quantum numbers s in odd-even nuclei is expanded in terms of a basis of the form $a^\dagger_{\tau\mu}|A,Rt,r\rangle$. The wave function $|A,Rt,r\rangle$ is an eigenfunction of the nuclear Hamiltonian for the even-even core state with angular momentum Rt and a set of additional quantum numbers labeled r. The expansion coefficients $u_{Is(\sigma_{\tau\mu},R,r)}$ are defined as

$$\langle A+1,IK,s|a^\dagger_{\tau\mu}|A,Rt,r\rangle=\langle j_\mu m_\mu Rt|IK\rangle u_{Is(\sigma_{\tau\mu},R,r)}. \tag{6}$$

An analogous expansion $\tilde{a}_{\tau\mu}|A,Rt,r\rangle$ is used for core-hole coupling with the coefficients $v_{Is(\sigma_{\tau\mu},R,r)}$ defined by

$$\langle A-1,IK,s|\tilde{a}_{\tau\mu}|A,Rt,r\rangle=\langle j_\mu m_\mu Rt|IK\rangle v_{Is(\sigma_{\tau\mu},R,r)}. \tag{7}$$

For odd-odd nuclei, a basis of the form $[a^\dagger_{\pi\lambda}\tilde{a}_{\nu\mu}]_{LM}|Z,N,Rt,r\rangle$ is used and the nuclear wave function is expanded with the coefficients $U_{Is(\sigma_{\pi\lambda},\sigma_{\nu\mu},L,R,r)}$ defined as

$$\langle Z+1,N-1,IK,s|[a^\dagger_{\pi\lambda}\tilde{a}_{\nu\mu}]_{LM}|Z,N,Rt,r\rangle=\langle LMRt|IK\rangle U_{Is(\sigma_{\pi\lambda},\sigma_{\nu\mu},L,R,r)}. \tag{8}$$

C. Application of the Kerman-Klein-Dönau-Frauendorf method

The Kerman-Klein-Dönau-Frauendorf method [12] was used in the current study to develop models for both odd-even and odd-odd nuclei. As outlined below, this is a linearized equation of motion method. The equations for both models are presented to emphasize the similarities in the formalism. Model parameters deduced for odd-even nuclei are expected to be directly applicable to the calculations for odd-odd nuclei.

The Heisenberg equations of motion for fermion creation and annihilation operators are

$$[H,a^\dagger_{\tau\mu}]=\varepsilon_{\tau\mu}a^\dagger_{\tau\mu}-\sum_{\tau'}\chi_{\tau\tau'}\sum_{\sigma_{\tau\mu'}}\frac{1}{\sqrt{2j_\mu+1}}q(\sigma_{\tau\mu},\sigma_{\tau\mu'})[a^\dagger_{\tau\mu'}Q(\tau')]_{j_\mu m_\mu}$$
$$-\frac{1}{2}\chi_{\tau\tau}\sum_{\mu'}\sum_{\sigma_{\tau\alpha}}\frac{1}{2j_\mu+1}q(\sigma_{\tau\mu},\sigma_{\tau\alpha})q(\sigma_{\tau\mu'},\sigma_{\tau\alpha})a^\dagger_{\tau\mu'}\delta_{j_\mu j_{\mu'}}\delta_{m_\mu m_{\mu'}}, \tag{9}$$

$$[H,\tilde{a}_{\tau\mu}]=-\varepsilon_{\tau\mu}\tilde{a}_{\tau\mu}+\sum_{\tau'}\chi_{\tau\tau'}\sum_{\sigma_{\tau\mu'}}\frac{1}{\sqrt{2j_\mu+1}}q(\sigma_{\tau\mu},\sigma_{\tau\mu'})[\tilde{a}_{\tau\mu'}Q(\tau')]_{j_\mu m_\mu}$$
$$-\frac{1}{2}\chi_{\tau\tau}\sum_{\mu'}\sum_{\sigma_{\tau\alpha}}\frac{1}{2j_\mu+1}q(\sigma_{\tau\mu},\sigma_{\tau\alpha})q(\sigma_{\tau\mu'},\sigma_{\tau\alpha})\tilde{a}_{\tau\mu'}\delta_{j_\mu j_{\mu'}}\delta_{m_\mu m_{\mu'}}. \tag{10}$$

These equations lead to the model for single-nucleon coupling. For the coupling of a proton particle and a neutron hole, the corresponding equation of motion is

[3]Note that, in the present paper K denotes the projection of the total angular momentum I on the quantization axis in the laboratory (not the intrinsic) reference frame.

$$[H,[a^{\dagger}_{\pi\lambda}\tilde{a}_{\nu\mu}]_{LM}]=(\varepsilon_{\pi\lambda}-\varepsilon_{\nu\mu})[a^{\dagger}_{\pi\lambda}\tilde{a}_{\nu\mu}]_{LM}$$

$$-\sum_{\tau'}\chi_{\pi\tau'}\sum_{\sigma_{\pi\lambda'}}\sum_{L'}(-)^{j_\lambda+j_\mu+L'}q(\sigma_{\pi\lambda},\sigma_{\pi\lambda'})\sqrt{2L'+1}\begin{Bmatrix} j_{\lambda'} & 2 & j_\lambda \\ L & j_\mu & L' \end{Bmatrix}[[a^{\dagger}_{\pi\lambda'}\tilde{a}_{\nu\mu}]_{L'}Q(\tau')]_{LM}$$

$$+\sum_{\tau'}\chi_{\nu\tau'}\sum_{\sigma_{\nu\mu'}}\sum_{L'}(-)^{j_\lambda+j_{\mu'}+L}q(\sigma_{\nu\mu},\sigma_{\nu\mu'})\sqrt{2L'+1}\begin{Bmatrix} j_{\mu'} & 2 & j_\mu \\ L & j_\lambda & L' \end{Bmatrix}[[a^{\dagger}_{\pi\lambda}\tilde{a}_{\nu\mu'}]_{L'}Q(\tau')]_{LM}$$

$$+\chi_{\pi\nu}\sum_{\sigma_{\pi\lambda'}}\sum_{\sigma_{\nu\mu'}}(-)^{j_{\lambda'}+j_\mu+L}q(\sigma_{\pi\lambda},\sigma_{\pi\lambda'})q(\sigma_{\nu\mu},\sigma_{\nu\mu'})\begin{Bmatrix} j_{\lambda'} & 2 & j_\lambda \\ j_\mu & L & j_{\mu'} \end{Bmatrix}[a^{\dagger}_{\pi\lambda'}\tilde{a}_{\nu\mu'}]_{LM}$$

$$-\frac{1}{2}\chi_{\pi\pi}\sum_{\sigma_{\pi\alpha}}\sum_{\sigma_{\pi\lambda'}}\frac{1}{2j_\lambda+1}q(\sigma_{\pi\lambda},\sigma_{\pi\alpha})q(\sigma_{\pi\lambda'},\sigma_{\pi\alpha})\delta_{j_\lambda j_{\lambda'}}[a^{\dagger}_{\pi\lambda'}\tilde{a}_{\nu\mu}]_{LM}$$

$$-\frac{1}{2}\chi_{\nu\nu}\sum_{\sigma_{\nu\alpha}}\sum_{\sigma_{\nu\mu'}}\frac{1}{2j_\mu+1}q(\sigma_{\nu\mu},\sigma_{\nu\alpha})q(\sigma_{\nu\mu'},\sigma_{\nu\alpha})\delta_{j_\mu j_{\mu'}}[a^{\dagger}_{\pi\lambda}\tilde{a}_{\nu\mu'}]_{LM}. \tag{11}$$

The basis defined by Eq. (6) was used to derive the eigenvalue equation for core-particle coupling

$$E_{Is(\sigma_{\tau\mu},R,r)}u_{Is(\sigma_{\tau\mu},R,r)}=\sum_{\sigma_{\tau\mu'},R',r'}H^{p}_{(\sigma_{\tau\mu},R,r)(\sigma_{\tau\mu'},R',r')}u_{Is(\sigma_{\tau\mu'},R',r')}. \tag{12}$$

The expression for the matrix element $H^{p}_{(\sigma_{\tau\mu},R,r)(\sigma_{\tau\mu'},R',r')}$ results from Eq. (9) when applying the wave function for an odd-even nucleus to its left-hand side and the wave function for an even-even core to its right-hand side

$$H^{p}_{(\sigma_{\tau\mu},R,r)(\sigma_{\tau\mu'},R',r')}=(E_{Rr}+\varepsilon_{\tau\mu})\delta_{\sigma_{\tau\mu}\sigma_{\tau\mu'}}\delta_{RR'}\delta_{rr'}-\chi(-)^{j_{\mu'}+R+I}\times\begin{Bmatrix} j_{\mu'} & 2 & j_\mu \\ R & I & R' \end{Bmatrix}q(\sigma_{\tau\mu},\sigma_{\tau\mu'})q(Rr,R'r'). \tag{13}$$

In the equations above, E_{Is} denotes the energy of the state with quantum numbers Is in an odd-even nucleus, E_{Rr} denotes the energy of the state with quantum numbers Rr in an even-even core, and $q(Rr,R'r')$ denotes the reduced matrix elements of the quadrupole operator between core states with quantum numbers Rr and $R'r'$. Equation (13) was derived under the assumption $\chi_{\pi\pi}=\chi_{\nu\nu}=\chi_{\pi\nu}=\chi$. The single-particle valence space for the current calculation is restricted to the $h_{11/2}$ orbital; in such an approximation the last term on the right-hand side of Eq. (9) can be neglected since it results only in an additive constant to the diagonal matrix elements of H^{p}. An analogous equation for a core-hole coupling model was derived from Eq. (10) using the basis defined in Eq. (7)

$$E_{Is(\sigma_{\tau\mu},R,r)}v_{Is(\sigma_{\tau\mu},R,r)}=\sum_{\sigma_{\tau\mu'},R',r'}H^{h}_{(\sigma_{\tau\mu},R,r)(\sigma_{\tau\mu'},R',r')}v_{Is(\sigma_{\tau\mu'},R',r')} \tag{14}$$

with the matrix H^{h} given by

$$H^{h}_{(\sigma_{\tau\mu},R,r)(\sigma_{\tau\mu'},R',r')}=(E_{Rr}-\varepsilon_{\tau\mu})\delta_{\sigma_{\tau\mu}\sigma_{\tau\mu'}}\delta_{RR'}\delta_{rr'}+\chi(-)^{j_{\mu'}+R+I}\times\begin{Bmatrix} j_{\mu'} & 2 & j_\mu \\ R & I & R' \end{Bmatrix}q(\sigma_{\tau\mu},\sigma_{\tau\mu'})q(Rr,R'r'). \tag{15}$$

When the wave function of the odd-odd nucleus is applied to the left-hand side of Eq. (11) and the wave function of the even-even core is applied to its right-hand side, the method leads to the model for core-particle-hole coupling. The eigenvalue equation for the $U_{Is(\sigma_{\pi\lambda},\sigma_{\nu\mu},L,R,r)}$ coefficients defined in Eq. (8) becomes

$$E_{Is(\sigma_{\pi\lambda},\sigma_{\nu\mu},L,R,r)}U_{Is(\sigma_{\pi\lambda},\sigma_{\nu\mu},L,R,r)}=\sum_{\sigma_{\pi\lambda'},\sigma_{\nu\mu'},L',R',r'}H^{ph}_{(\sigma_{\pi\lambda},\sigma_{\nu\mu},L,R,r)(\sigma_{\pi\lambda'},\sigma_{\nu\mu'},L',R',r')}U_{Is(\sigma_{\pi\lambda'},\sigma_{\nu\mu'},L',R',r')} \tag{16}$$

with the matrix H^{ph} defined by

$$
\begin{aligned}
&H^{ph}_{(\sigma_{\pi\lambda},\sigma_{\nu\mu},L,R,r)(\sigma_{\pi\lambda'},\sigma_{\nu\mu'},L',R',r')} \\
&\quad = (E_{Rr}+\varepsilon_{\lambda\pi}-\varepsilon_{\mu\nu})\,\delta_{\sigma_{\pi\lambda}\sigma_{\pi\lambda'}}\delta_{\sigma_{\nu\mu}\sigma_{\nu\mu'}}\delta_{LL'}\delta_{RR'}\delta_{rr'} \\
&\qquad -\chi(-)^{j_\lambda+j_\mu+R+I}\sqrt{2L+1}\sqrt{2L'+1}\begin{Bmatrix} j_{\lambda'} & 2 & j_\lambda \\ L & j_\mu & L' \end{Bmatrix}\begin{Bmatrix} L' & 2 & L \\ R & I & R' \end{Bmatrix} q(\sigma_{\pi\lambda},\sigma_{\pi\lambda'})\,\delta_{\sigma_{\nu\mu}\sigma_{\nu\mu'}} q(Rr,R'r') \\
&\qquad +\chi(-)^{j_\lambda+j_{\mu'}+L+L'+R+I}\sqrt{2L+1}\sqrt{2L'+1}\begin{Bmatrix} j_{\mu'} & 2 & j_\mu \\ L & j_\lambda & L' \end{Bmatrix}\begin{Bmatrix} L' & 2 & L \\ R & I & R' \end{Bmatrix}\delta_{\sigma_{\pi\lambda}\sigma_{\pi\lambda'}} q(\sigma_{\nu\mu},\sigma_{\nu\mu'}) q(Rr,R'r') \\
&\qquad +\chi(-)^{j_{\lambda'}+j_\mu+L}\begin{Bmatrix} j_{\mu'} & 2 & j_\mu \\ j_\lambda & L & j_{\lambda'} \end{Bmatrix} q(\sigma_{\pi\lambda},\sigma_{\pi\lambda'}) q(\sigma_{\nu\mu},\sigma_{\nu\mu'})\,\delta_{LL'}\delta_{RR'}\delta_{rr'}\,. \qquad (17)
\end{aligned}
$$

Equation (17) was developed under the same assumption as for Eqs. (13) and (15).

The parameters required to calculate matrix elements given by Eqs. (13), (15), and (17) are the energies and reduced matrix elements of the quadrupole operator for single-particle states and for the core. The model, therefore, can be conveniently applied to studies of valence particle coupling with various cores. The current calculations consider coupling with a triaxial rotor [14]. The single-particle basis was limited to the unique parity $h_{11/2}$ orbitals for both the valence proton and neutron. Equations (12), (14), and (16) were solved numerically, which provides the energies and wave functions for odd-even and odd-odd nuclei. The choice of model parameters is discussed in Sec. IV.

D. Electromagnetic properties

The wave functions resulting from the diagonalization of Eqs. (12), (14), or (16) were used to compute the reduced matrix elements of the $M1$ and $E2$ operators. In the case of core-particle coupling, the reduced matrix element of the operator $\mathcal{M}(\Lambda)$ is given by

$$
\begin{aligned}
&\langle I's',A+1||\mathcal{M}(\Lambda)||Is,A+1\rangle \\
&\quad = \sqrt{2I+1}\sqrt{2I'+1}\Bigg[\sum_{\sigma_{\tau\mu}}\sum_{Rr,R'r'}(-)^{j_\mu+R+I'+\Lambda}\begin{Bmatrix} I' & \Lambda & I \\ R & j_\mu & R' \end{Bmatrix}\langle R'r'||\mathcal{M}(\Lambda)||Rr\rangle u_{Is(\sigma_{\tau\mu},R,r)} u_{I's'(\sigma_{\tau\mu},R',r')} \\
&\qquad +\sum_{\sigma_{\tau\mu},\sigma_{\tau\mu'}}\sum_{R,r}(-)^{j_{\mu'}+R+I+\Lambda}\begin{Bmatrix} I' & \Lambda & I \\ j_\mu & R & j_{\mu'} \end{Bmatrix}\langle\sigma_{\tau\mu'}||\mathcal{M}(\Lambda)||\sigma_{\tau\mu}\rangle u_{Is(\sigma_{\tau\mu},R,r)} u_{I's'(\sigma_{\tau\mu'},R,r)}\Bigg]. \qquad (18)
\end{aligned}
$$

The corresponding formula for the core-hole coupling is

$$
\begin{aligned}
&\langle I's',A-1||\mathcal{M}(\Lambda)||Is,A-1\rangle \\
&\quad = \sqrt{2I+1}\sqrt{2I'+1}\Bigg[\sum_{\sigma_{\tau\mu}}\sum_{Rr,R'r'}(-)^{j_\mu+R+I'+\Lambda}\begin{Bmatrix} I' & \Lambda & I \\ R & j_\mu & R' \end{Bmatrix}\langle R'r'||\mathcal{M}(\Lambda)||Rr\rangle v_{Is(\sigma_{\tau\mu},R,r)} v_{I's'(\sigma_{\tau\mu},R',r')} \\
&\qquad +\sum_{\sigma_{\tau\mu},\sigma_{\tau\mu'}}\sum_{R,r}c(-)^{j_{\mu'}+R+I+\Lambda}\begin{Bmatrix} I' & \Lambda & I \\ j_\mu & R & j_{\mu'} \end{Bmatrix}\langle\sigma_{\tau\mu'}||\mathcal{M}(\Lambda)||\sigma_{\tau\mu}\rangle v_{Is(\sigma_{\tau\mu},R,r)} v_{I's'(\sigma_{\tau\mu'},R,r)}\Bigg], \qquad (19)
\end{aligned}
$$

where

$$
c=\begin{cases} -1 & \text{for electric multipoles} \\ +1 & \text{for magnetic multiples} \end{cases} \qquad (20)
$$

is a factor related to the transformation properties of the matrix element of the $\mathcal{M}(\Lambda)$ operator under particle-hole conjugation as discussed in Sec. 3.1b of Ref. [8].

For proton-particle and neutron-hole coupling to the core, the corresponding reduced matrix element is given by

$$\langle I's',Z+1,N-1||\mathcal{M}(\Lambda)||Is,Z+1,N-1\rangle$$
$$=\sqrt{2I+1}\sqrt{2I'+1}\Bigg[\sum_{\sigma_{\pi\lambda},\sigma_{\nu\mu}}\sum_{L}\sum_{Rr,R'r'}(-)^{L+R+I'+\Lambda}\begin{Bmatrix}I' & \Lambda & I\\ R & L & R'\end{Bmatrix}$$
$$\times\langle R'r'||\mathcal{M}(\Lambda)||Rr\rangle U_{Is(\sigma_{\pi\lambda},\sigma_{\nu\mu},L,R,r)}U_{I's'(\sigma_{\pi\lambda},\sigma_{\nu\mu},L,R',r')}$$
$$+\sum_{\sigma_{\pi\lambda},\sigma_{\pi\lambda'}}\sum_{\sigma_{\nu\mu}}\sum_{L,L'}\sum_{R,r}(-)^{j_{\lambda'}+j_\mu+L+L'+R+I}\sqrt{2L+1}\sqrt{2L'+1}\begin{Bmatrix}L' & \Lambda & L\\ j_\lambda & j_\mu & j_{\lambda'}\end{Bmatrix}\begin{Bmatrix}I' & \Lambda & I\\ L & R & L'\end{Bmatrix}$$
$$\times\langle\sigma_{\pi\lambda'}||\mathcal{M}(\Lambda)||\sigma_{\pi\lambda}\rangle U_{Is(\sigma_{\pi\lambda},\sigma_{\nu\mu},L,R,r)}U_{I's'(\sigma_{\pi\lambda'},\sigma_{\nu\mu},L',R,r)}$$
$$+\sum_{\sigma_{\pi\lambda}}\sum_{\sigma_{\nu\mu},\sigma_{\nu\mu'}}\sum_{L,L'}\sum_{R,r}c(-)^{j_\lambda+j_\mu+R+I}\sqrt{2L+1}\sqrt{2L'+1}\begin{Bmatrix}L' & \Lambda & L\\ j_\mu & j_\lambda & j_{\mu'}\end{Bmatrix}\begin{Bmatrix}I' & \Lambda & I\\ L & R & L'\end{Bmatrix}$$
$$\times\langle\sigma_{\nu\mu'}||\mathcal{M}(\Lambda)||\sigma_{\nu\mu}\rangle U_{Is(\sigma_{\pi\lambda},\sigma_{\nu\mu},L,R,r)}U_{I's'(\sigma_{\pi\lambda},\sigma_{\nu\mu'},L',R,r)}\Bigg]. \tag{21}$$

E. Scalar operators of angular momenta

The wave function of a state in an odd-odd nucleus provided by the model contains information about the coupling of the three angular momenta: the angular momentum of the core R, the angular momentum of the proton j_π, and the angular momentum of the neutron j_ν. Information specific to the orientation of these individual angular momenta can be partially separated out by employing calculated expectation values for scalar product operators involving these three vectors. The scalar operators considered in this study are as follows:

$$\langle Is|R^2|Is\rangle=\sum_{\sigma_{\pi\lambda}}\sum_{\sigma_{\nu\mu}}\sum_{L}\sum_{R}\sum_{r}R(R+1)U^2_{Is(\sigma_{\pi\lambda},\sigma_{\nu\mu},L,R,r)}, \tag{22}$$

$$\langle Is|j_\pi j_\nu|Is\rangle=\frac{1}{2}\sum_{\sigma_{\pi\lambda}}\sum_{\sigma_{\nu\mu}}\sum_{L}\sum_{R}\sum_{r}\{L(L+1)-j_\pi(j_\pi+1)-j_\nu(j_\nu+1)\}U^2_{Is(\sigma_{\pi\lambda},\sigma_{\nu\mu},L,R,r)} \tag{23}$$

$$\langle Is|Rj_\pi|Is\rangle=\sum_{\sigma_{\pi\lambda}}\sum_{\sigma_{\nu\mu}}\sum_{L,L'}\sum_{R}\sum_{r}(-)^{j_\lambda+j_\nu+R+I}\times\sqrt{R(R+1)}\sqrt{j_\lambda(j_\lambda+1)}\sqrt{2R+1}\times\sqrt{2j_\lambda+1}\sqrt{2L+1}\sqrt{2L'+1}\begin{Bmatrix}L' & 1 & L\\ j_\lambda & j_\mu & j_\lambda\end{Bmatrix}\times\begin{Bmatrix}L' & 1 & L\\ R & I & R\end{Bmatrix}U_{Is(\sigma_{\pi\lambda},\sigma_{\nu\mu},L,R,r)}\times U_{Is(\sigma_{\pi\lambda},\sigma_{\nu\mu},L',R,r)}, \tag{24}$$

$$\langle Is|Rj_\nu|Is\rangle=\sum_{\sigma_{\pi\lambda}}\sum_{\sigma_{\nu\mu}}\sum_{L,L'}\sum_{R}\sum_{r}(-)^{j_\lambda+j_\mu+R+I}(-)^{L+L'}\times\sqrt{R(R+1)}\sqrt{j_\mu(j_\mu+1)}\sqrt{2R+1}\times\sqrt{2j_\mu+1}\sqrt{2L+1}\sqrt{2L'+1}\begin{Bmatrix}L' & 1 & L\\ j_\mu & j_\lambda & j_\mu\end{Bmatrix}\times\begin{Bmatrix}L' & 1 & L\\ R & I & R\end{Bmatrix}U_{Is(\sigma_{\pi\lambda},\sigma_{\nu\mu},L,R,r)}\times U_{Is(\sigma_{\pi\lambda},\sigma_{\nu\mu},L',R,r)}. \tag{25}$$

F. The orientation operator

An important part of these calculations is to investigate the chiral interpretation, namely, that the nearly degenerate band members observed for the $\pi h_{11/2}\nu^{-1}h_{11/2}$ configuration in triaxial odd-odd nuclei (^{132}La) result from the two orientations, left- and right-handed systems, in which the perpendicular angular momenta j_π, j_ν, and R can couple to the total angular momentum I. The operator

$$\sigma=(\vec{j}_\pi\times\vec{j}_\nu)\cdot\vec{R} \tag{26}$$

is used below to examine the orientation of these vectors. Its expectation value would peak for three mutually perpendicular angular momenta in the intrinsic frame; it has opposite signs for the left-handed and right-handed systems. This operator changes sign under time reversal.

The operator σ may be expressed in terms of the coupling of spherical tensors [26]

$$\sigma=i\sqrt{6}[[\mathbf{j}_\pi\otimes\mathbf{j}_\nu]_1\otimes\mathbf{R}]_0=i\mathbf{V}, \tag{27}$$

where $\mathbf{j}_\pi$, $\mathbf{j}_\nu$, and $\mathbf{R}$ are spherical tensors of rank 1 (vectors) and $\mathbf{V}$ is a spherical tensor of rank 0 (scalar). The reduced

matrix element of the **V** operator between the basis states for the core-particle-hole coupling model is given by

$$\begin{aligned}\langle I'\sigma_{\pi\lambda'},\sigma_{\nu\mu'},L',R',r'||\mathbf{V}||I\sigma_{\pi\lambda},\sigma_{\nu\mu},L,R,r\rangle &= \delta_{I\,I'}\delta_{\lambda\lambda'}\delta_{\mu\,\mu'}\delta_{R\,R'}\delta_{r\,r'}(-)^{L'+R+I} \\ &\times\sqrt{6}\sqrt{2L+1}\sqrt{2L'+1}\sqrt{2j_\lambda+1} \\ &\times\sqrt{2j_\mu+1}\sqrt{2R+1}\sqrt{j_\lambda(j_\lambda+1)}\sqrt{j_\mu(j_\mu+1)}\sqrt{R(R+1)} \\ &\times\begin{Bmatrix} L' & 1 & L \\ R & I & R\end{Bmatrix}\begin{Bmatrix} L' & L & 1 \\ j_\mu & j_\mu & 1 \\ j_\lambda & j_\lambda & 1\end{Bmatrix}. \end{aligned} \tag{28}$$

The matrix element defined by Eq. (28) changes sign when transposed. As a consequence, the expectation value of the **V** and σ operators for any state in the laboratory reference frame is zero; therefore, the orientation of states in the laboratory reference frame is never specified. If, however, for a given spin I there exist states $|I\mathcal{R}\rangle$ and $|I\mathcal{L}\rangle$, which come from the right-handed and the left-handed intrinsic states, respectively, the restoration of time reversal requires that the physical states are [16]

$$|I+\rangle=\frac{1}{\sqrt{2}}(|I\mathcal{R}\rangle+|I\mathcal{L}\rangle),$$

$$|I-\rangle=\frac{i}{\sqrt{2}}(|I\mathcal{R}\rangle-|I\mathcal{L}\rangle). \tag{29}$$

For nearly degenerate levels,

$$\langle I+||\sigma||I-\rangle=i\langle I+||\mathbf{V}||I-\rangle\approx i\langle I\mathcal{R}||\sigma||I\mathcal{R}\rangle. \tag{30}$$

The normalized orientation parameter, which varies between ±1, is defined as

$$\tilde{\sigma}=\tilde{\sigma}_{\mathcal{R}}=\frac{\langle I\mathcal{R}|\sigma|I\mathcal{R}\rangle}{\sqrt{\langle I\mathcal{R}|j_\pi^2|I\mathcal{R}\rangle}\sqrt{\langle I\mathcal{R}|j_\nu^2|I\mathcal{R}\rangle}\sqrt{\langle I\mathcal{R}|R^2|I\mathcal{R}\rangle}}=-\tilde{\sigma}_{\mathcal{L}}. \tag{31}$$

It is related to matrix elements for the states in the laboratory system by

$$\tilde{\sigma}\approx\frac{\sqrt{2}\langle I+|\mathbf{V}|I-\rangle}{j(j+1)\sqrt{\langle I+|R^2|I+\rangle+\langle I-|R^2|I-\rangle}} \tag{32}$$

with $j=5.5$ for the $\pi h_{11/2}\nu^{-1}h_{11/2}$ configuration. In the calculations discussed below, the wave functions for $|I+\rangle$ and $|I-\rangle$ states are assumed to be those provided by the core-particle-hole coupling model for the nearly degenerate pairs of states.

IV. MODEL PARAMETERS FOR THE $A\sim130$ REGION

A. The core: Calculations for ^{130}Ba and ^{132}Ba

The focus of the current study is to investigate gross structure features of the core-particle-hole coupling in odd-odd nuclei; a triaxial rotor [14] is used, therefore, for the core. A triaxial core with $\gamma\sim-30°$ (Lund convention[4]) was a prediction of the TAC calculations in the intrinsic frame [15], although total Routhian surface [27] calculations suggest that nuclei in this mass region are γ soft to some degree. The use of a triaxial rotor seems to be justified by the experimental results of Refs. [1–5], which imply relatively rigid triaxiality required for the existence of $\pi h_{11/2}\nu^{-1}h_{11/2}$ chiral partners. This most likely results from the fact that, for odd-odd nuclei, particle-hole configurations stabilize triaxial deformations due to the opposing shape-driving forces. The mathematical simplicity of a triaxial rotor for the core has advantages in these studies.

TABLE II. Parameters of the models used in the current study: quadrupole deformation parameters β and γ, mass parameter B for the moment of inertia and the coupling constant χ for quadrupole-quadrupole interactions.

Nucleus	β	γ	B ($\hbar^2$/MeV)	χ (MeV/b^2)
^{130}Ba	0.220	24°	95	
^{131}Ba	0.21	32°	95	9
^{132}Ba	0.192	26°	95	
^{131}La	0.23	20°	95	9
^{132}La	0.23	21°	95	9
^{133}La	0.21	20°	95	9
^{134}Pr	0.25	35°	95	9

The Hamiltonian for the triaxial rotor is given by

$$H=\sum_{k=1}^{3}\frac{R_k^2}{2J_k}, \tag{33}$$

where R_k and J_k denote projections of the angular momentum operator and moments of inertia in the intrinsic coordinate frame, respectively. The three irrotational-flow-like moments of inertia are given by the equation [28]

$$J_k=4B\beta^2\sin^2\left(\gamma-\frac{2k\pi}{3}\right),\quad k=1,2,3, \tag{34}$$

which is consistent with the corresponding formula of Ref. [6]. The model has three parameters: quadrupole deformation β, triaxiality γ, and mass parameter B.

Deformation parameters $\beta=0.220$, $\gamma=24°$, and $\beta=0.192$, $\gamma=26°$ were extracted for ^{130}Ba and ^{132}Ba, respectively, from the $B(E2,2_1^+\rightarrow0_1^+)$ values and the ratios of the energies of the first and the second 2^+ states [29,30] (the model parameters for all of the nuclei investigated in the current study are summarized in Table II). In both Ba nuclei, good agreement between the calculated and experimental energies for the excited states in the yrast band was observed for a mass parameter $B=95\hbar^2$/MeV. Comparisons between

[4]Note that the triaxiality parameter γ as defined by the Lund convention has the opposite sign to that defined in Ref. [14]. The convention of Ref. [14] is consistently applied in the discussion below.

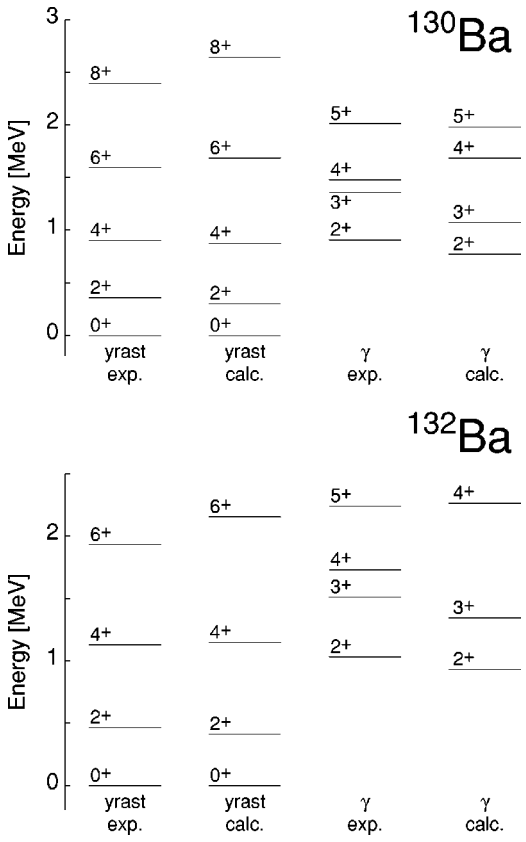

FIG. 4. Comparisons between energies of excited states in the yrast and γ bands in ^{130}Ba and ^{132}Ba with those calculated for a rigid triaxial rotor. See Table II for the model parameters. The experimental data are taken from Refs. [29] and [30] for ^{130}Ba and ^{132}Ba, respectively.

selected experimental and calculated level energies are presented in Fig. 4 while those for transition rates are presented in Table III.

It is apparent from Fig. 4 that the energies for the high-spin yrast states in ^{130}Ba and ^{132}Ba are overestimated using a triaxial rotor. This is a consequence of the constant moment of inertia assumed in the calculations while experimentally moments of inertia in the $A\sim130$ region increase with increasing spin (rotational frequency). More sophisticated parametrizations for the moment of inertia, for example, a variable moment of inertia (VMI) [31], yield usually better agreement with experimental data. Calculations using the VMI have been investigated; however, in the present study, a constant moment of inertia is assumed for simplicity. Additionally, in ^{130}Ba and ^{132}Ba, a crossing is observed near spin $\sim10\hbar$ with the resulting *S*-band built on an excited two-quasineutron $(h_{11/2})^2$ configuration as established by a *g*-factor measurement of Ref. [32]. This crossing may perturb the energies of the yrast levels with spins lower than 10^+, but is blocked in the rotational bands of the odd-odd nuclei studied. Therefore, the constant moment of inertia is expected to approximate the core properties in ^{132}La better than the ^{132}Ba nucleus itself.

As shown in Fig. 4, the calculated and experimental energies in the γ bands have slightly different trends. In the calculations, the states with spins 2^+ and 3^+ or 4^+ and 5^+ are clustered together, whereas experimentally the clustering is observed for the states with spin 3^+ and 4^+. This feature was pointed out in Ref. [33] as a characteristic that differentiates between γ-rigid and γ-vibrational models for even-even nuclei. More sophisticated approaches, such as those of Refs. [34–36] based on the Bohr Hamiltonian, the interacting boson model, or the general collective model, respectively, can be used to calculate the core properties. A more detailed core description will be considered in future calculations.

B. Core-particle and -hole coupling: Calculations for ^{131}La, ^{133}La, and ^{131}Ba

The core-particle coupling model with a $\chi=9$ MeV/b^2 coupling constant for the quadrupole-quadrupole interaction was applied for the calculation of the $h_{11/2}$-band properties in odd-proton ^{131}La and ^{133}La. The coupling constant when scaled by a factor $A^{-5/3}$ is consistent with $\chi\sim11$ MeV/b^2 used in a similar study in the $A\sim110$ region [37] where good agreement between experimental and calculated energies was observed for the $h_{11/2}$ band of ^{111}Te. In the current studies, the basis for the core consisted of states up to spin 16^+ in the yrast band and states up to spin 13^+ in the γ band. The best overall agreement between the calculations and experimental data was achieved for cores with $\beta=0.23$ and $\gamma=20°$, and $\beta=0.21$ and $\gamma=20°$ for ^{131}La and ^{133}La, respectively, for the mass parameter $B=95\hbar^2$/MeV (see Table II); the values of β and γ for the cores are slightly higher and smaller, respectively, than those extracted for the corresponding even

TABLE III. Comparison between transition rates in ^{130}Ba and ^{132}Ba with those calculated for a rigid triaxial rotor. See Table II for the model parameters. The experimental data are taken from Refs. [29] and [30] for ^{130}Ba and ^{132}Ba, respectively.

	^{130}Ba		^{132}Ba	
	Exp	Calc	Exp	Calc
$B(E2,2_1^+\rightarrow0_1^+)$ $[e^2b^2]$	0.26(3)	0.229	0.175(13)	0.174
$B(E2,2_2^+\rightarrow0_1^+)$ $[e^2b^2]$		0.005	0.015(2)	0.005
$B(E2,2_2^+\rightarrow2_1^+)$ $[e^2b^2]$		0.153	0.591(60)	0.166
$\frac{B(E2,2_2^+\rightarrow2_1^+)}{B(E2,2_2^+\rightarrow0_1^+)}$		31	39(6)	31

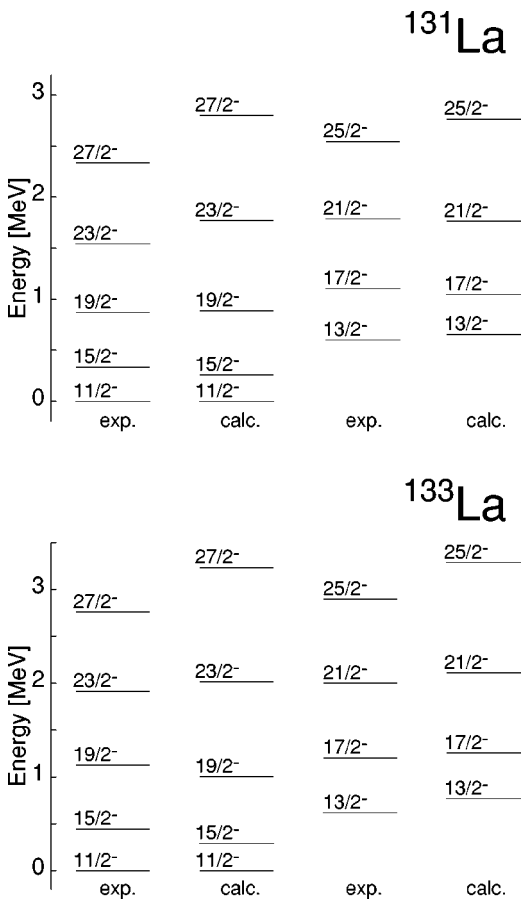

FIG. 5. Comparisons between energies of excited states in the yrast band in ^{131}La and ^{133}La with those calculated for a $\pi h_{11/2}$ particle coupled to a rigid triaxial rotor. See Table II for the model parameters. The experimental data are taken from Refs. [38] and [39] for ^{131}La and ^{133}La, respectively.

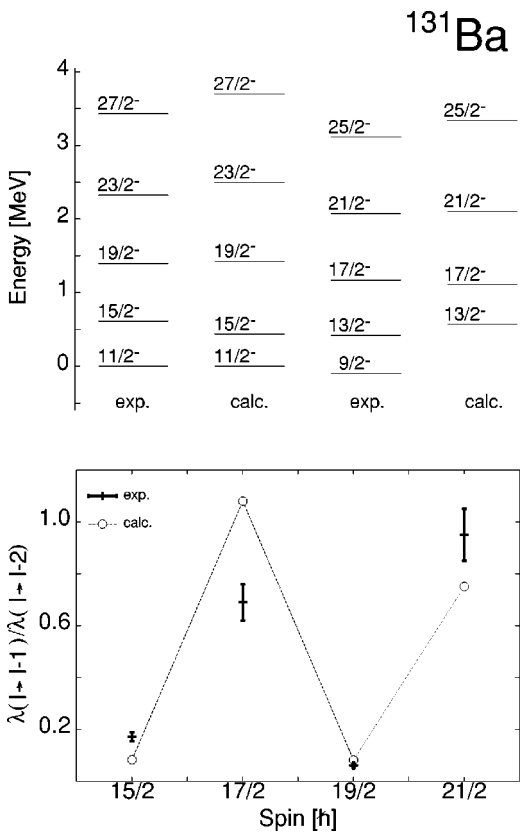

FIG. 6. (Top) Comparison between energies of excited states in the yrast band in ^{131}Ba with those calculated for a $\nu h_{11/2}$ hole coupled to a rigid triaxial rotor. (Bottom) Comparison between branching ratios in the yrast band in ^{131}Ba with those calculated for a $\nu h_{11/2}$ hole coupled to a rigid triaxial rotor. See Table II for the model parameters. The experimental data are taken from Ref. [38].

Ba isotopes. This is consistent with the prolate-deformation driving property of the $\pi h_{11/2}$ orbital in this mass region.

A core-hole coupling model was applied to calculate the properties of the $h_{11/2}$ band in odd-neutron ^{131}Ba with the same coupling constant for the quadrupole-quadrupole interaction, and the same mass parameter for the core as used for core-particle coupling (see Table II). The best overall agreement between the calculated and experimental level energies was observed for a triaxial core with $\beta=0.21$ and $\gamma=32°$. The larger triaxiality relative to that for the corresponding core is consistent with the oblate driving properties of the $\nu h_{11/2}$ hole orbital.

These calculations for odd-even nuclei are not sensitive to the single-particle energies of the $h_{11/2}$ states. The reduced matrix element of the quadrupole operator $q(h_{11/2},h_{11/2})=-0.3636$ b used for the coupling of the $h_{11/2}$ proton and neutron was determined assuming radial wave functions of a harmonic oscillator [28]. The reduced matrix elements of the magnetic dipole operator $\langle \pi h_{11/2}||\mathcal{M}(M1)||\pi h_{11/2}\rangle=25.1\mu_{\mathrm{N}}$ and $\langle \nu h_{11/2}||\mathcal{M}(M1)||\nu h_{11/2}\rangle=-4.33\mu_{\mathrm{N}}$ needed to evaluate $M1$ transition rates in odd-even nuclei were calculated assuming a 0.6 spin attenuation factor.

Comparisons between the experimental [38,39] and calculated level energies are presented in Fig. 5 for the odd-proton La nuclei and in the top panel of Fig. 6 for odd-neutron ^{131}Ba. The systematic discrepancy observed in Fig. 5 for the states at higher spins reflects a similar discrepancy for the core. For ^{131}Ba, energies for all the states observed experimentally are well reproduced except for the $9/2^-$ state. A core-quasiparticle coupling model and/or a more elaborate core description are needed to reproduce the properties of this $9/2^-$ state. A larger single-particle basis that includes $f_{7/2}$ and $h_{9/2}$ orbitals may also be necessary.

The experimental and calculated transition rates for ^{131}La are in good agreement as presented in Table IV. For ^{131}Ba

TABLE IV. Comparison between transition rates in ^{131}La and ^{133}La with those calculated for a $\pi h_{11/2}$ particle coupling with rigid triaxial rotor. See Table II for the model parameters. The experimental data for ^{131}La are taken from Ref. [38].

	^{131}La		^{133}La	
	Exp	Calc	Exp	Calc
$B(E2,15/2^-\rightarrow 11/2^-)$ [e^2b^2]	0.346(11)	0.329		0.277
$B(E2,19/2^-\rightarrow 15/2^-)$ [e^2b^2]	0.330(30)	0.361		0.305

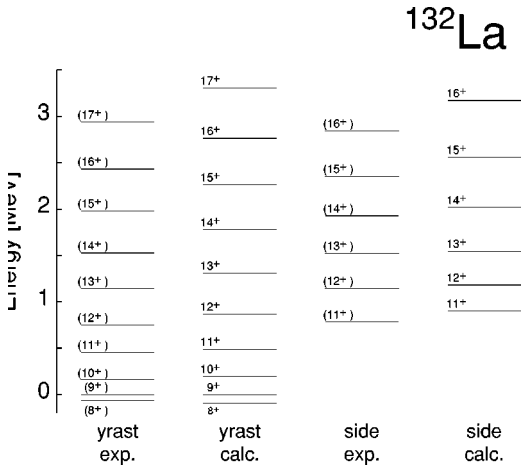

FIG. 7. Comparison between energies of excited states in the partner band in ^{132}La with those calculated for $\pi h_{11/2}\nu^{-1}h_{11/2}$ particle-hole coupling with a rigid triaxial rotor (see Table II for the model parameters). Theoretical states are shown only when the corresponding experimental states are known.

the experimental and theoretical branching ratios are compared in the bottom panel of Fig. 6. These branching ratios were calculated using theoretical $B(M1)$ and $B(E2)$ reduced transition probabilities and experimental energies (the $E2$ contributions to the $\Delta I=1$ $17/2^- \rightarrow 15/2^-$ and $21/2^- \rightarrow 19/2^-$ transitions are substantial). The magnitude and staggering of the experimental branching ratios are correctly reproduced.

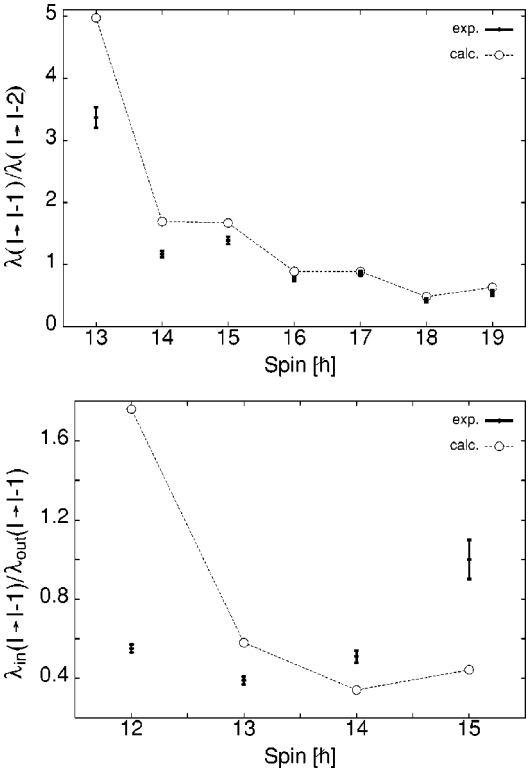

FIG. 8. (Top) Comparison between branching ratios in the yrast band in ^{132}La with those calculated for $\pi h_{11/2}\nu^{-1}h_{11/2}$ particle-hole coupling with a rigid triaxial rotor. (Bottom) Comparison between experimental and calculated branching ratios for the $\Delta I=1$ transitions in the partner band and the $\Delta I=1$ transitions between the partner band and the yrast band in ^{132}La. See Table II for the model parameters.

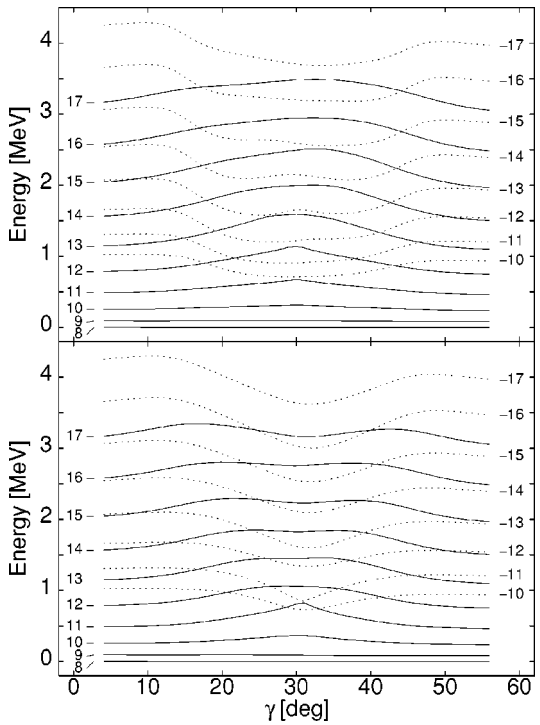

FIG. 9. Excitation energies for the states forming the yrast band (solid lines) and the partner band (dashed lines) in an odd-odd nucleus calculated with the core-particle-hole coupling model as a function of triaxiality of the core. The basis for the calculations shown in the top panel includes the yrast band and the γ band for the core. The basis for the calculations shown in the bottom panel includes only the yrast band for the core. States are labeled with spin and have positive parity. See text for the model parameters.

C. Core-particle-hole coupling: Calculation for ^{132}La

The core-particle-hole coupling model was used to calculate the properties of the $\pi h_{11/2}\nu^{-1}h_{11/2}$ bands in odd-odd ^{132}La observed in the current experiment. The parameters were those established above (see Table II) including the reduced matrix elements of the quadrupole and magnetic moment operators for single-particle states. The best overall agreement between the calculated and experimental level energies and between the branching ratios was observed for a triaxial core with $\beta=0.23$ and $\gamma=21°$. This value for β is comparable to that of ^{131}La but is larger than that for ^{133}La. This is consistent with the larger collectivity expected for the core as the neutron Fermi level decreases toward the midshell. The deduced triaxiality for the ^{132}La core is closer to the triaxiality of the odd-proton La isotopes rather than to that of the odd-neutron ^{131}Ba. This may suggest that in the case of ^{132}La the driving force exerted by the valence $h_{11/2}$ neutron hole is not large enough to overcome the prolate driving force of the valence $h_{11/2}$ proton. It should be noted, however, that these values of the model parameters are extracted without pairing interactions for the valence nucleons and are expected to be altered slightly in paired calculations.

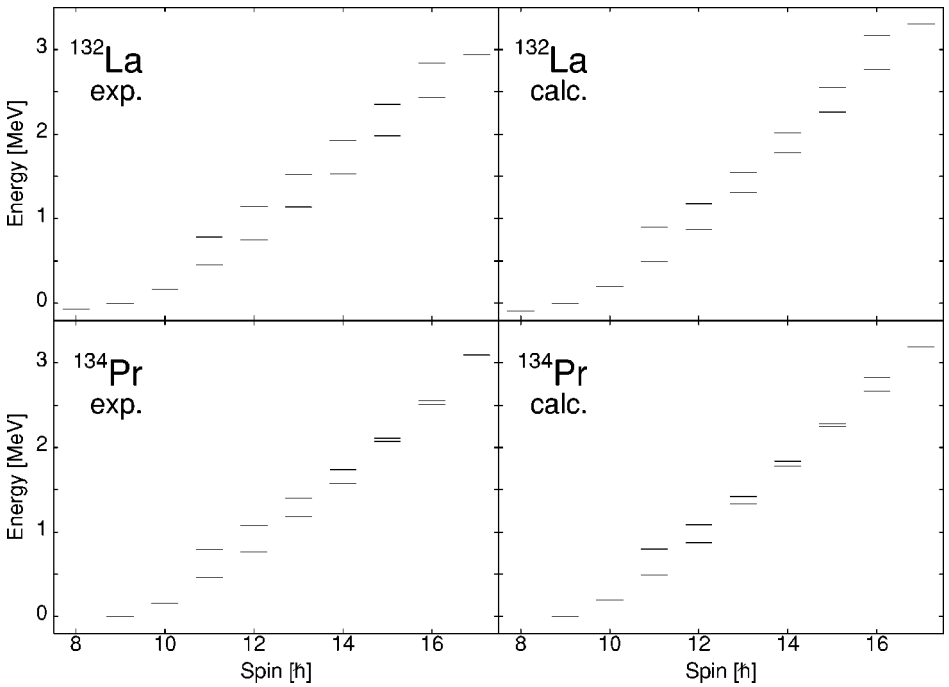

FIG. 10. Comparisons between energies of observed $\pi h_{11/2}\nu^{-1}h_{11/2}$ states in ^{132}La (top) and ^{134}Pr (bottom) with those calculated for $\pi h_{11/2}\nu^{-1}h_{11/2}$ particle-hole coupling with a rigid triaxial rotor. See Table II for the model parameters.

The experimental and calculated level energies are compared in Fig. 7. Both the yrast band and the partner band are reproduced in the calculations. Comparisons between the experimental and theoretical branching ratios are presented in Fig. 8. The branching ratios were calculated using theoretical $B(M1)$ and $B(E2)$ reduced transition probabilities and experimental energies. The top panel of Fig. 8 presents the branching ratios for the intraband transitions in the yrast band. A good general agreement is observed; however, the calculated branching ratios are systematically larger at low spins. The bottom panel of Fig. 8 presents the branching ratios for the $\Delta I=1$ transitions in the partner band and the $\Delta I=1$ transitions between the partner band and the yrast band; the order of the magnitude for these branching ratios is correctly reproduced. The agreement between the calculation and the experimental data is significantly worse, especially for the branching ratios, if a spin (7^+), rather than the (8^+), was assigned to the bandhead of the yrast band as was proposed in Ref. [18].

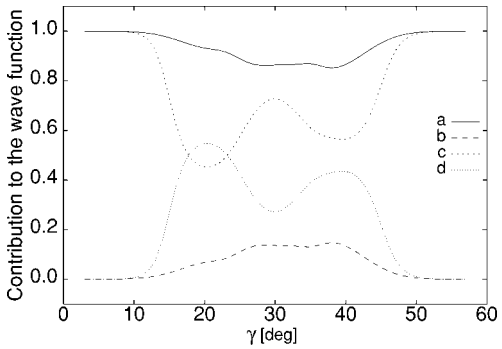

FIG. 11. Line *a*: Contribution of the core yrast states to the wave function of the yrast 14^+ state. Line *b*: Contribution of the core γ states to the wave function of the yrast 14^+ state. Line *c*: Contribution of the core yrast states to the wave function of the 14^+ state in the partner band. Line *d*: Contribution of the core γ states to the wave function of the 14^+ state in the partner band. The calculations were done for a core with quadrupole deformation $\beta=0.23$.

V. DISCUSSION

A. Role of the core triaxiality and the γ-band coupling

The core-particle-hole coupling model with $\chi=9$ MeV/b^2, the core parameters $\beta=0.23$ and $B=95\hbar^2$/MeV, and single-particle parameters discussed above was applied to study the role of the core triaxiality in odd-odd nuclei. The basis for these calculations includes the yrast band and the γ band of the core as discussed in Sec. IV A. Excitation energies calculated for states in the yrast and the partner bands of a generic odd-odd nucleus are shown in the top panel of Fig. 9. It is observed in the calculations that the 12^+, 13^+, 14^+, and 15^+ states of both bands are separated by an energy of several hundred keV for the core with $\gamma\sim 0°$ and $\gamma\sim 60°$, but become nearly degenerate for a triaxial core with $\gamma\sim 30°$. Experimentally, such degeneracy is observed for ^{134}Pr [23], which is an $N=75$ isotone of ^{132}La. The best agreement between the calculated and the experimental energies for the bands in ^{134}Pr was observed for a core with $\beta=0.25$ and $\gamma\sim 35°$. Figure 10 summarizes the results of the calculations in comparison to the experimental data from ^{132}La and ^{134}Pr.

To further investigate the role of coupling to the γ band, the calculations were repeated for $\beta=0.23$ and the standard model parameters with a basis that includes only the yrast states of the core. The resulting excitation energies for states in the yrast band and the partner band in an odd-odd nucleus are shown in the bottom panel of Fig. 9. Both sets of calculations presented in Fig. 9 show the same trend, although degeneracy is observed only for the 11^+ state in the calculations with the basis not including the core γ band.

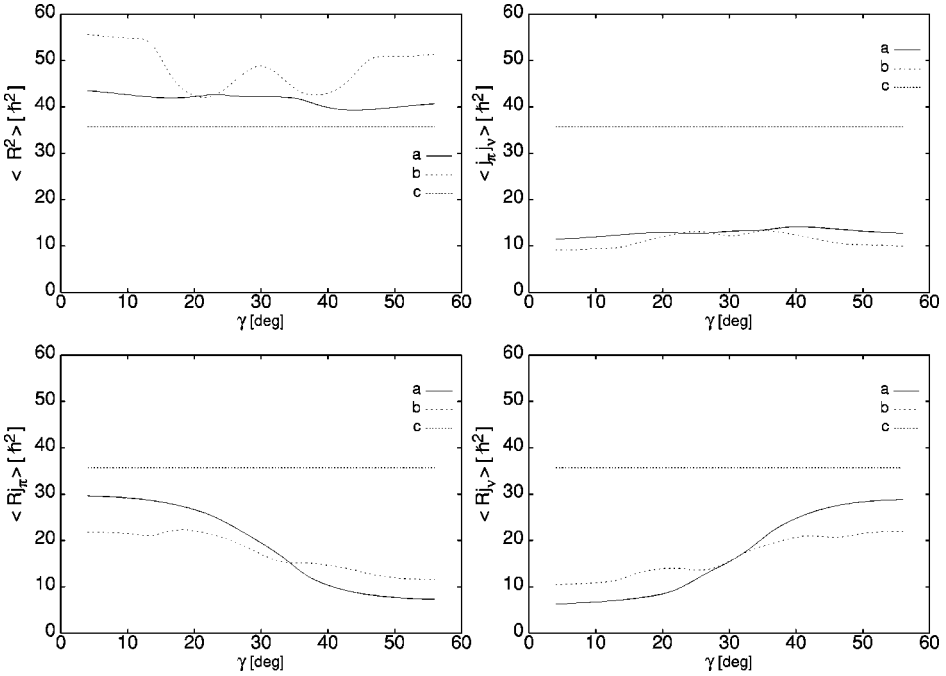

FIG. 12. Expectation values for the scalar operators defined in Sec. III E: (top left) $\langle R^2\rangle$, (top right) $\langle j_\pi j_\nu\rangle$, (bottom left) $\langle Rj_\pi\rangle$, and (bottom right) $\langle Rj_\nu\rangle$, calculated as a function of triaxiality for the core with $\beta=0.23$ and for (line *a*) the yrast 14^+ state and (line *b*) the 14^+ state in the partner band. The horizontal line *c* gives the expectation value for the $\langle j_\pi^2\rangle=\langle j_\nu^2\rangle$ operator for the $h_{11/2}$ orbital.

The wave functions for the states in an odd-odd nucleus calculated with the basis including the core γ band were inspected to identify contributions from the yrast band and γ band of the core. The results for the 14^+ states shown in Fig. 11 indicate that for a triaxial core with $\gamma\sim30°$, the contribution from the γ band of the core is $\sim10\%$ for the yrast 14^+ state (line *b*) and $\sim30\%$ for the 14^+ state in the partner band (line *d*). It is further observed in Fig. 11 that for core deformations around $\gamma=30°$, the contributions due to the γ-band coupling decrease. It is concluded, therefore, that although the coupling of the valence nucleons with the γ band of the core does play a role in these detailed calculations, some other mechanism, which predominantly involves coupling with the core yrast states, is needed to explain the level degeneracy for odd-odd triaxial nuclei. The chiral hypothesis offers such a mechanism.

B. Coupling of angular momenta

The scalar operators defined in Sec. III E were used to investigate the coupling of the angular momenta of the core, the proton particle, and the neutron hole to the total angular momentum. The expectation values of these operators calculated as a function of the triaxiality for the core with $\beta=0.23$ for the yrast 14^+ state and the 14^+ state in the partner band are shown in Fig. 12.

According to the calculations presented in the top left panel of Fig. 12, the average core contribution to the total angular momentum for both 14^+ states (lines *a* and *b*) is comparable ($R\sim6.5\hbar$) to the contributions from the valence proton and valence neutron $h_{11/2}$ orbital (line *c*). The results for the $\langle j_\pi j_\nu\rangle$ shown in the top right panel of Fig. 12 (lines *a* and *b*) indicates that the coupling of the angular momenta for the valence proton and valence neutron changes only slightly with the core triaxiality. If the effective angle between the proton and neutron angular momenta is defined through $\cos\zeta=\langle j_\pi j_\nu\rangle/\sqrt{\langle j_\pi^2\rangle\langle j_\nu^2\rangle}$, the calculations predict near perpendicular coupling with $\zeta\sim75°$.

The calculations presented in the left bottom panel of Fig. 12 show a distinct dependence of $\langle Rj_\pi\rangle$ (lines *a* and *b*) on the core triaxiality. For near prolate shapes with $\gamma\sim0°$ the $\langle Rj_\pi\rangle$ is smaller but comparable to $\langle R\rangle\langle j_\pi\rangle$, which indicates a preference for alignment of the angular momentum of the proton particle along the angular momentum of the core. For near oblate shapes with $\gamma\sim60°$, $\langle Rj_\pi\rangle$ is significantly smaller than $\langle R\rangle\langle j_\pi\rangle$, which indicates a preference for alignment of the angular momentum of the proton particle along a direction perpendicular to the angular momentum of the core. The opposite conclusions can be reached for the neutron hole.

For triaxial shapes with $\gamma\sim30°$, the expectation values for $\langle j_\pi j_\nu\rangle$, $\langle Rj_\pi\rangle$, and $\langle Rj_\nu\rangle$ calculated for 14^+ states in the yrast and in the partner bands are nearly equal. This suggests similar perpendicular geometries for the coupling of angular momenta. If the effective angles between the core angular momentum and the angular momentum of the valence nucleon are defined through $\cos\psi=\langle Rj_\pi\rangle/\sqrt{\langle R^2\rangle\langle j_\pi^2\rangle}$ and $\cos\xi=\langle Rj_\nu\rangle/\sqrt{\langle R^2\rangle\langle j_\nu^2\rangle}$, the calculations predict $\psi\sim\xi\sim65°$.

The results presented above are consistent with the interpretation based on the chiral hypothesis. Degenerate levels are indeed observed for states that have a core contribution to the total angular momentum comparable to the angular momentum of the valence proton and the valence neutron. For these doublet states, the calculated effective angles between the three angular momenta involved indicate similar geometries with near perpendicular coupling. The scalar operators discussed above do not define, however, the handedness of the system. The wave functions provided by the core-particle-hole coupling model with the standard set of parameters were used, therefore, to evaluate the expectation value

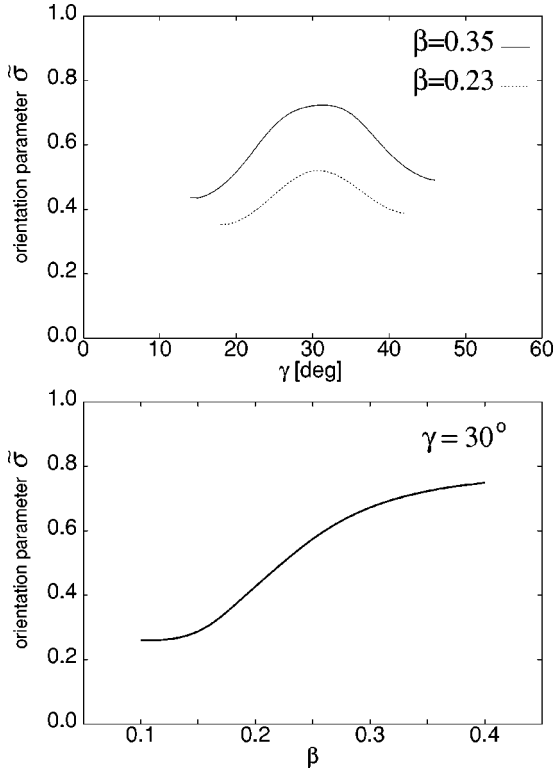

FIG. 13. (Top) Orientation parameter $\tilde{\sigma}$ calculated as a function of triaxiality γ for $\beta=0.23$ and $\beta=0.35$. (Bottom) Orientation parameter $\tilde{\sigma}$ calculated as a function of β for $\gamma=30°$.

of the orientation parameter $\tilde{\sigma}$ defined in Sec. III F. The upper panel of Fig. 13 presents the results at spin 14^+ as a function of triaxiality for $\beta=0.23$ and $\beta=0.35$. In both cases the orientation parameter peaks for $\gamma=30°$ and decreases as the core becomes axially symmetric. (For a classical mechanical system, $\tilde{\sigma}=1$ for mutually perpendicular vectors yielding an aplanar orientation, while $\tilde{\sigma}=0$ would represent a planar orientation.) This trend correlates very well with the level degeneracy observed in the upper panel of Fig. 9. The lower panel of Fig. 13 presents the orientation parameter calculated as a function of β for a core with fixed $\gamma=30°$. The orientation is predicted to increase as core deformation increases. Both trends shown in Fig. 13 are in full agreement with those expected from the chiral hypothesis.

C. Role of the core β deformation

As shown above, not only the $\gamma\sim30°$ triaxiality but also a relatively large β is essential to observe the degenerate states in odd-odd nuclei. Indeed, in the $A\sim130$ region, two of the three mutually perpendicular angular momenta are provided by the valence proton particle coupled to the short axis of the core and the valence neutron hole coupled to the long axis of the core. This coupling is expected to occur only if the axes of the core are sufficiently different in length. For a triaxial shape with $\gamma=30°$, the ratio of the short to long axis is $s/l\sim0.9$ for $\beta=0.1$, $s/l\sim0.8$ for $\beta=0.2$, and $s/l\sim0.7$ for $\beta=0.3$.

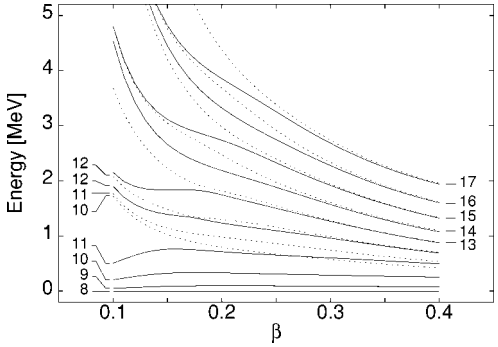

FIG. 14. Excitation energies for the states forming the yrast band (solid lines) and the partner band (dashed lines) in an $A=130$ odd-odd nucleus calculated with the core-particle-hole coupling model as a function of β deformation for the triaxial core with $\gamma=30°$. States are labeled with spin and have positive parity. See text for the model parameters.

The core-particle-hole coupling model with standard parameters was used to investigate the role of the core deformation in detail. Energies for states in the yrast and the partner bands calculated as a function of β for a fixed $\gamma=30°$ triaxiality are shown in Fig. 14. At a deformation of $\beta=0.35$, the levels with a common spin between 13^+ and 19^+ in the yrast and in the partner bands have energies that differ by less than 50 keV; these energies start to diverge for $\beta<0.23$ and are hundreds of keV apart for deformations smaller than $\beta\sim0.17$. This trend correlates very well with that shown for the orientation parameter in the lower panel of Fig. 13. The effective angles between the angular momenta of the proton, the neutron, and the core at $\beta=0.35$ are $\zeta\sim\psi\sim\xi\sim80°$. These results are in full agreement with the chiral hypothesis.

At high deformations, the calculations show that the core γ band still contributes up to 20% to the wave function for the degenerate states. If the γ band is removed from the core basis, the levels with a common spin between 10^+ and 17^+ in both bands have energies that differ by less then 100 keV. The γ band in the core seems, therefore, to play a role even at high deformations, but is not essential to generate levels with similar excitation energies in these triaxial odd-odd nuclei.

VI. SUMMARY AND CONCLUSIONS

Information regarding the excited states built on the $\pi h_{11/2}\nu^{-1}h_{11/2}$ configuration in ^{132}La was extended in the current experiment from the previous work in Ref. [18]. The $\pi h_{11/2}\nu^{-1}h_{11/2}$ yrast band and the partner band identified in the current studies show striking similarities when compared to the corresponding bands in ^{134}Pr, which is an $N=75$ isotone of ^{132}La. The interpretation proposed in Ref. [6] for these structures as resulting from the coupling of the orthogonal angular momenta vectors in triaxial odd-odd nuclei into right- and left-handed systems of opposite chirality was investigated with the use of a phenomenological core-particle-hole coupling model. The Hamiltonian for the model included single-particle terms and quadrupole-quadrupole interactions. The eigenvalues for the Hamiltonian were calcu-

lated using the Kerman-Klein-Dönau-Frauendorf method that provides a convenient way to study the valence particle coupling with various cores. The coupling to a triaxial rotor was investigated in the current study. The model parameters were fitted to reproduce the properties of the yrast bands in even-even nuclei and the $h_{11/2}$ bands in odd-even nuclei in the $A=130$ region, which resulted in good descriptions for five $_{56}$Ba and $_{57}$La nuclides within a consistent set of values. Good agreement between the experimental energies and branching ratios in odd-odd ^{132}La and those calculated using the core-particle-hole coupling model was achieved with the use of these parameters.

The results of the calculations for an odd-odd nucleus were analyzed for the configuration with an $h_{11/2}$ proton particle and an $h_{11/2}$ neutron hole as a function of the core β and γ deformations. The resulting coupling of the angular momenta of the core, of the valence proton, and of the valence neutron was studied by evaluating the expectation values of the $\langle j_\pi j_\nu \rangle$, $\langle R j_\pi \rangle$, and $\langle R j_\nu \rangle$ operators and the orientation operator $\tilde{\sigma}$. The particle angular momentum was observed to align with the core angular momentum for the prolate cores and in the direction perpendicular to the core angular momentum for the oblate cores; the opposite was observed for the hole. In the calculations, the alignment was stronger for larger β.

In triaxial odd-odd nuclei with $\gamma \sim 30°$ and moderate deformation β for configurations with a high-j particle and a high-j hole, the model predicts the existence of levels with the same spin/parity and energies within ~ 100 keV. Nearly orthogonal coupling of angular momenta vectors for these doublets is suggested by the calculated expectation values for the $\langle j_\pi j_\nu \rangle$, $\langle R j_\pi \rangle$, and $\langle R j_\nu \rangle$ operators while the existence of the right- and the left-handed systems in the intrinsic, body-fixed reference frame is revealed via the calculated expectation value for the orientation operator $\tilde{\sigma}$. The energies for the doublets are observed to diverge as γ approaches $0°$ or $60°$ with levels becoming ~ 1 MeV apart for axially symmetric cores. For a fixed $\gamma \sim 30°$ triaxiality, the energies for the doublets are observed to converge as the β deformation of the core increases. At a deformation of $\beta \sim 0.35$ and $\gamma \sim 30°$, the levels with a common spin between 13^+ and 19^+ were calculated to be less than 50 keV apart for the $\pi h_{11/2} \nu^{-1} h_{11/2}$ configuration.

The calculated spins for the doublet states are dependent not only on the single-particle configuration and core deformation, but also on the collective basis assumed for the core in the calculations. The energy difference for the doublets was found to increase and the doublets appeared at lower spins when the γ band was removed from the core collective basis for $\gamma \sim 30°$. In the calculations with the γ band included in the core collective basis, the contribution of the core γ states to the wave function of the states in an odd-odd nucleus was observed to be smaller than 30% at $\gamma \sim 30°$ and $\beta \sim 0.2$. The γ-band states still contribute at higher deformations ($\sim 20\%$ for $\gamma \sim 30°$ and $\beta \sim 0.35$), which suggests that the degrees of freedom associated with the γ band are important for detailed calculations, although not essential to generate the doublet states.

The results summarized above are consistent with those of Refs. [1–6] and with the proposed interpretation for the observed $\pi h_{11/2} \nu^{-1} h_{11/2}$ bands as resulting from the coupling of the mutually perpendicular angular momenta of the core, proton particle, and neutron hole into two systems that differ by intrinsic chirality. Other possible explanations discussed in these papers for the observed doublet structures are ruled out as inconsistent with the experimental data. The model reported in the current paper can be easily applied to study effects of the core γ softness as well as influences of the specific proton-neutron interactions on the structure of these bands.

ACKNOWLEDGMENTS

The authors would like to kindly acknowledge the motivating discussion with Professor S. Frauendorf as well as Professor P. Semmes and Professor Jing-ye Zhang regarding the core-particle-hole coupling model and the interpretation of the results. This work was supported in part by U.S. NSF under award PHY-0098793. One of us (S.G.R.) would like to acknowledge a partial support by Polish Committee for Scientific Research (KBN) under Contract No. P03B 014 21.

[1] K. Starosta, T. Koike, C.J. Chiara, D.B. Fossan, D.R. LaFosse, A.A. Hecht, C.W. Beausang, M.A. Caprio, J.R. Cooper, R. Krücken, J.R. Novak, N.V. Zamfir, K.E. Zyromski, D.J. Hartley, D.L. Balabanski, Jing-ye Zhang, S. Frauendorf, and V.I. Dimitrov, Phys. Rev. Lett. **86**, 971 (2001).

[2] T. Koike, K. Starosta, C.J. Chiara, D.B. Fossan, and D.R. LaFosse, Phys. Rev. C **63**, 061304(R) (2001).

[3] D.J. Hartley, L.L. Riedinger, M.A. Riley, D.L. Balabanski, F.G. Kondev, R.W. Laird, J. Pfohl, D.E. Archer, T.B. Brown, R.M. Clark, M. Devlin, P. Fallon, I.M. Hibbert, D.T. Joss, D.R. LaFosse, P.J. Nolan, N.J. O'Brien, E.S. Paul, D.G. Sarantites, R.K. Sheline, S.L. Shepherd, J. Simpson, R. Wadsworth, Jing-ye Zhang, P.B. Semmes, and F. Dönau, Phys. Rev. C **64**, 031304(R) (2001).

[4] A.A. Hecht, C.W. Beausang, K.E. Zyromski, D.L. Balabanski, C.J. Barton, M.A. Caprio, R.F. Casten, J.R. Cooper, D.J. Hartley, R. Krücken, D. Meyer, H. Newman, J.R. Novak, E.S. Paul, N. Pietralla, A. Wolf, N.V. Zamfir, Jing-ye Zhang, and F. Dönau, Phys. Rev. C **63**, 051302(R) (2001).

[5] R.A. Bark, A.M. Baxter, A.P. Byrne, G.D. Dracoulis, T. Kibédi, T.R. McGoram, and S.M. Mullins, Nucl. Phys. **A691**, 577 (2001).

[6] S. Frauendorf and J. Meng, Nucl. Phys. **A617**, 131 (1997).

[7] J. Meyer-ter-Vehn, Nucl. Phys. **A249**, 111 (1975).

[8] A. Bohr and B. Mottelson, *Nuclear Structure* (Benjamin, New York, 1975).

[9] F. Dönau and S. Frauendorf, Phys. Lett. **71B**, 263 (1977).

[10] Ch. Droste, D. Chlebowska, J. Dobaczewski, F. Dönau, A.

Kerek, G. Leander, J. Srebrny, and W. Waluś, Nucl. Phys. **A341**, 98 (1980).
[11] F. Dönau and U. Hagemann, Z. Phys. A **293**, 31 (1979).
[12] A. Klein, Phys. Rev. C **63**, 014316 (2000).
[13] F. Dönau, in *Microscopic Approaches to Nuclear Structure Calculations*, edited A. Covello (Societa Italiana di Fisica, Sorrento, 1986); (private communication).
[14] A.S. Davydov and B.F. Fillipov, Nucl. Phys. **8**, 237 (1958).
[15] V.I. Dimitrov, S. Frauendorf, and F. Dönau, Phys. Rev. Lett. **84**, 5732 (2000).
[16] K. Starosta, T. Koike, C.J. Chiara, D.B. Fossan, and D.R. LaFosse, Nucl. Phys. **A682**, 375c (2001).
[17] D.C. Radford, Nucl. Instrum. Methods Phys. Res. A **361**, 297 (1995).
[18] J.R.B. Oliveira, L.G.R. Emediato, M.A. Rizzutto, R.V. Ribas, W.A. Seale, M.N. Rao, N.H. Medina, S. Botelho, and E.W. Cybulska, Phys. Rev. C **39**, 2250 (1989).
[19] A. Krämer-Flecken, T. Morek, R.M. Lieder, W. Gast, G. Hebbinghaus, H.M. Jeger, and W. Urban, Nucl. Instrum. Methods Phys. Res. A **275**, 333 (1989); K.S. Krane, R.M. Steffen, and R.M. Wheeler, Nucl. Data Tables **11**, 351 (1973).
[20] B. Harmatza and T.H. Handley, Nucl. Phys. **A191**, 497 (1972).
[21] G.H. Fuller, J. Phys. Chem. Ref. Data **5**, 835 (1976).
[22] Y. Liu, J. Lu, Y. Ma, S. Zhou, and H. Zheng, Phys. Rev. C **54**, 719 (1996); Y. Liu, J. Lu, Y. Ma, G. Zhao, H. Zheng, and S. Zhou, *ibid.* **58**, 1849 (1998).
[23] C.M. Petrache, D. Bazzacco, S. Lunardi, C. Rossi Alvarez, G. de Angelis, M. De Poli, D. Bucurescu, C.A. Ur, P.B. Semmes, and R. Wyss, Nucl. Phys. **A597**, 106 (1996); C.M. Petrache, G. de Angelis, D. Bucurescu, M. Ivascu, D. Bazzacco, and S. Lunardi, Z. Phys. A **344**, 227 (1992).
[24] C.W. Beausang, L. Hildingsson, E.S. Paul, W.F. Piel, Jr., N. Xu, and D.B. Fossan, Phys. Rev. C **36**, 1810 (1987).
[25] P.R. Sala, N. Blasi, G. Lo Bianco, A. Mazzoleni, R. Reinhardt, K. Schiffer, K.P. Schmittgen, G. Siems, and P. von Brentano, Nucl. Phys. **A531**, 383 (1991).
[26] D. A. Varshalovich, A. N. Moskalev, and V. K. Khersonskii, *Quantum Theory of Angular Momentum* (World Scientific, New Jersey, 1988).
[27] R. Wyss, J. Nyberg, A. Johnson, R. Bengtsson, and W. Nazarewicz, Phys. Lett. B **215**, 211 (1988).
[28] J. M. Eisenberg and W. Greiner, *Nuclear Theory*, Nuclear Models Vol. 1 (North Holland, Amsterdam, 1987).
[29] Yu.V. Sergeenkov, Nucl. Data Sheets **58**, 765 (1989).
[30] Yu.V. Sergeenkov, Nucl. Data Sheets **65**, 277 (1992).
[31] M.A.J. Mariscotti, G. Scharff-Goldhaber, and B. Buck, Phys. Rev. **178**, 1864 (1969).
[32] P. Das, R.G. Pillay, V.V. Krishnamurthy, S.N. Mishra, and S.H. Devare, Phys. Rev. C **53**, 1009 (1996).
[33] W. Lieberz, A. Dewald, W. Frank, A. Gelberg, W. Krips, D. Lieberz, R. Wirowski, and P. von Brentano, Phys. Lett. B **240**, 38 (1990).
[34] L. Próchniak, K. Zając, K. Pomorski, S.G. Rohoziński, and J. Srebrny, Nucl. Phys. **A648**, 181 (1999).
[35] O. Vogel, P. Van Isacker, A. Gelberg, P. von Brentano, and A. Dewald, Phys. Rev. C **53**, 1660 (1996).
[36] P. Petkov, A. Dewald, and W. Andrejtscheff, Phys. Rev. C **51**, 2511 (1995).
[37] K. Starosta, C.J. Chiara, D.B. Fossan, T. Koike, D.R. LaFosse, G.J. Lane, J.M. Sears, J.F. Smith, A.J. Boston, P.J. Nolan, E.S. Paul, A.T. Semple, M. Devlin, D.G. Sarantites, I.Y. Lee, and A.O. Macchiavelli, Phys. Rev. C **61**, 034308 (2000).
[38] Yu.V. Sergeenkov, Yu.L. Khazov, T.W. Burrows, and M.R. Bhat, Nucl. Data Sheets **72**, 487 (1994).
[39] S. Rab, Nucl. Data Sheets **75**, 491 (1995).